SSRG International Journal of Electronics and Communication Engineering
ISSN: 2348-8549/ https://doi.org/10.14445/23488549/IJECE-V11I10P115

Volume 11 Issue 10, 186-201, October 2024

Original Article

Charef Approximation Method for Fractional Order System Models Using Hybrid FMINCON-Mayfly Optimization Algorithm

Sanjay Ambadas Patil[1], Uday Pandit Khot[2]

[1,2]*St. Francis Institute of Technology, Maharashtra, India.*

[1]*Corresponding Author : sapatil1969@gmail.com*

Received: 15 August 2024 Revised: 16 September 2024 Accepted: 15 October 2024 Published: 30 October 2024

Abstract *- Fractional order calculus in modelling and control applications has been increasingly popular in every scientific field due to its versatility and superiority in various instances. These methods present advantages in frequency response approximation. However, real-world engineering applications require more accurate time responses to implement FO operators. Consequently, the article proposed FO systems' rational integer order approximate transfer function. This will positively contribute to the realization performance of FO system models in real-world applications. A pole and zero model of the Charef rational approximation method is proposed on a fractional-order transfer function. The poles of the approximate model are unrelated to the order of the integrator. This feature shows the benefits of extending the algorithm to the systems containing various fractional orders. Moreover, numerical examples are given to show the wide applicability of this method and to illustrate the acceptable accuracy for approximations. Further, time responses of FMINCON-based FO derivative models are improved by the Mayfly Optimization Algorithm (MOA). This study analyses the convergence behaviour and magnitude error metrics of the different order FO to improve magnitude response. In addition, the research proposed to optimize the Simulated Annealing (SA) algorithm for the determination of optimal hyper-parameters with custom target values to improve magnitude response. The proposed work is implemented using Matlab software. The analysis process involves selecting key parameters such as fractional order, optimization algorithm settings, and convergence criteria. Validation methods include comparing the results from the proposed approaches with analytical solutions and employing metrics like magnitude error to assess accuracy. The numerical simulations of various test cases are conducted to confirm the effectiveness and robustness of the model. Comparing the analytical and actual solutions demonstrates that the proposed approaches effectively and efficiently investigate complicated nonlinear models. Furthermore, the proposed methodologies control and manipulate the achieved better solutions in a very useful way, providing a simple process to adjust and control the convergence regions of the series solution.*

Keywords *- Fractional Order System, Charef approximation, FMINCON, Mayfly optimization, Magnitude error metrics, Simulated annealing, Hyper-parameters.*

1. Introduction

The discipline of engineering and applied sciences has recently shown a strong interest in Fractional Partial Differential Equations (FPDE). The FPDE is found to be a useful tool in the interpretation and modelling of many problems that arise in physics, biology, and applied mathematics. Its extensive applicability in real-world problems is described by this equation. As a result, academics have given substantial attention to solving FPDEs and differential equations. Because most FPDE lacks exact analytic solutions, approximate and numerical approaches are frequently used [1, 2]. When used to describe the inherited and memory characteristics of various materials and systems, the fractional derivative is an excellent contrivance. Modelling actual materials' electrical and mechanical properties and those of rocks, signal processing, and numerous other fields is done using Fractional Differential Equations (FDE) [3]. A novel epidemiological model that considered both integer and fractional order operators was created in addition to understanding the dynamics of measles transmission. A singular solution to the Caputo fractional model exists in the positively invariant area [4]. A more exact attenuation characteristic of analogue filters has recently been achieved by applying the theoretical idea of fractional calculus that deals with the generalization of the classical concepts of differentiation and integration. Because the traditional Laplacian operator s has been generalized to the Fractional-Order (FO) form s^{α}, where $\alpha \in (0,1)$, this is

conceivable, which gives system modelling extra degrees of freedom [5]. The ideas of fractal and fractional differentiation have been merged to create new differentiation operators. The generalized Mittag-Leffler function, the power law, and exponential decay were used as the three kernels for constructing the new operators. The two new operators' parameters are the first, which is regarded as fractional order, and the second is the fractal dimension. A highly effective numerical approach is developed in [6] to simulate several chaotic attractors to solve the models. The Charef approximation method for fractional-order system models has shown promise, yet significant challenges remain in effectively integrating fractional elements into practical applications. Existing optimization techniques often fall short in addressing the complexities of these models, particularly when it comes to achieving optimal performance in real-world scenarios. This research identifies a gap in robust optimization strategies that can seamlessly incorporate fractional-order dynamics. The proposed hybrid Fmincon-Mayfly optimization algorithm aims to bridge this gap, enhancing the accuracy and efficiency of fractional-order system modelling.

[7] defines a novel computational method for solving FDE using the Atangana-Baleanu derivative and the Laguerre polynomial. The operational matrices for fractional integration and fractional integral differentiation are developed for this purpose using Laguerre polynomials. The generated operational matrices and collocation points reduce the FDEs to a set of linear or nonlinear algebraic equations. A bound on the error is derived for the operational matrix of the fractional integration. The mathematical formulation of fractional pantograph differential equations is presented in [8] using a brand-new class of functions known as fractional-order Alpert multiwavelet functions. Consideration is given to the Caputo-type fractional derivative. The fractional-order Alpert multiwavelet functions are used in this instance to create the Riemann-Liouville fractional operational matrix of integration. High-order and fractional differentiators, both of which have continuously tunable orders, are used in signal processing [9]. To enhance a mathematical representation of a two-mass system with a long shaft and concentrated parameters, the Caputo-Fabrizio operator is applied, and its application is evaluated based on the general theory of fractional order derivatives and integrals. Ordinary fractional-order differential equations are used to explain such systems. Additionally, it is widely known that an elastic mechanical wave that travels down a long, stiff shaft in a drive transmission would cause the distribution of the angular velocities in time and space, the angle at which the shaft is rotating, and the elastic moment to slow down [10, 11]. The fractional order model and its synchronization are also included. They are based on an optimized fractional order sliding mode controller and are not analytically solved; instead, they are solved using genetic algorithms, which can produce intelligent solutions with an objective function and some additive unknown parameters [12, 13].

The calculation of the fractional-order integrator and equivalent may result in infinite complexity, which is a key challenge for fractional-order element implementations. The concept of the various FOPID controller implementation strategies has been provided in [14, 15]. However, one negative side effect of adopting classical approximations of the fractional-order elements in the FOPID controllers is the steady-state inaccuracy. Latif and Kumarasamy demonstrate how applying different optimization strategies lowers steady-state inaccuracy. The ideal set of these parameters was successfully obtained using many optimization techniques, including the Genetic Algorithm (GA), Bacterial Foraging Optimization (BFO) algorithm, Artificial Bee Colony (ABC) algorithm, and many more [16-18]. The execution of such techniques might reveal their primary distinctions (i.e., the realization of the controller's integral and the differential components) [19, 20].

AVR maintains a synchronous generator's voltage as the main excitation system controller at a specific level. The proposed controller is simulated within various scenarios, and its performance is compared with those of an optimally designed PID controller. A recently Simulated Annealing is presented to tune the hyperparameters, it can significantly improve the magnitude response of the system by analyzing the convergence behaviour and magnitude error metrics of the different order FO. The rest of the work is described as follows: Section 2 portrays the literature survey of the research, and Section 3 demonstrates the definition of the research problem and its motivation. Section 4 reveals the proposed research methodology, Section 5 elucidates the experimentation and result discussion, and the conclusion of the research work is established in Section 6.

2. Literature Survey

Aguila Camacho N et al. [21] extended to situations where system states are influenced by a bounded non-parametric disturbance. Simulation studies are conducted with various representative plants to be controlled, demonstrating that fractional orders and levels of switching error can be observed in most cases. Valencia-Ponce M A. et al. [22] utilized to plan adders and subtractors, while the multiplication of variables is achieved through development. The paper demonstrates that the simulation results, which scale the mathematical model to amplitudes below ±1, align well with the outcomes obtained using 180 nm CMOS IC technology. Charef A et al. [23] obtained from the time response of the proposed analogue dynamical model. The efficiency and accuracy of the numerical evaluation results for the proposed are compared with those of Lorenzo and Hartley using an illustrative example. Bettou K et al. [24] compared those achieved with the classical PIDA controller using various design methods from the literature. The

simulation results further indicate a substantial improvement in the performance and robustness of the closed-loop system when employing the proposed fractional order controller design. Lassoued A. et al. [25] implied that even a slight variation in the initial conditions could lead to a significant difference in the final stages of hyperchaotic systems. Simulations demonstrate that the system can generate various attractors, including equilibrium points, limit cycles, and hyperchaotic attractors.

Adigintla S et al. [26] planned for the FOPI manager to be integrated into the rotor field-oriented control algorithm for the Induction Motor (IM). Hardware learning is conducted using a research laboratory HIL stage to validate the robustness of the planned FOPI manager estimate method. Duddeti B B et al. [27] assessed using several performance metrics and time response characteristics. Finally, inverse substitution transforms the concentrated number direction sample rear into a CFS. Boucherma D et al. [28] round these roles to derive rational purposes in the forms.

This transformation was accomplished by applying the concept of fractional commensurate order, making it directly relevant to real-world physics. Emad S et al. [29] focused on their scale fault, level fault, and application difficulty. The examined techniques include CFE, Padé, Charef, and approximations using the MATLAB curve-fitting tool. Yüce A et al. [30] proposed a method that is compared to existing studies in the literature regarding time and frequency responses. Results indicate that it offers improved model approximation performance and achieves a lower-order model.

3. Research Problem Definition and Motivation

Fractional calculus is gaining popularity because it enables more precise modelling of real systems and enhances system solutions that cannot be reached with integer order system models. Because of this, a wide range of real-world applications are identified in this fractional calculus. To find more reliable answers to various scientific and engineering issues, fractional order system models make it possible to represent real-world systems more accurately, and fractional order modelling has been used. Limited-band and integer-order approximations are frequently used to create fractional-order transfer functions due to the enormous computational load of the ideal realization of fractional-order elements. The approximate fractional order models may impair the usability of optimal control tuning techniques, which is a significant side effect of such a non-ideal fractional order controller function realization for control applications. This fundamental difficulty prohibits engineering problems from fully utilizing the benefits of optimal fractional order behaviour (Tepljakov et al. 2018). Approximate integer-order models, which can approximate responses of fractional order elements in constrained operating ranges, were developed to deal with these difficulties and implement fractional order elements with tolerable processing overhead. In control practice, these approximate models were frequently used for the non-ideal realization of FOPID controllers. Because analytical tuning approaches primarily require an ideal realization of FOPID controller functions, the performance of approximate models inherently degrades the practical performance of optimal tuning methods. Consequently, real-world control performance is significantly lower than the theoretically attainable ideal control performance when fractional order elements are implemented roughly. For these reasons, the real-world performance of fractional-order control systems in applications should be a major issue when choosing an appropriate approximate model to implement fractional-order transfer functions.

4. Proposed Research Methodology

In time domain analysis, components or elements of a power system with known characteristics in the frequency domain are modelled using approximated rational functions. Based on the assumption that the dynamics are lumped and time-invariant, traditional differential equations and integer order transfer functions are typically used to describe linear circuits and systems. However, many dynamical systems are better modelled by fractional calculus, with the interaction of the variables being modelled by fractional integration and/or fractional differentiation than the conventional integer order calculus. With the help of experimental data, the current work suggests a generalized method for identifying fractional order systems in the frequency domain.

Many methods have been proposed to accurately compute models for transient studies by fitting the frequency response to rational functions. In this work, a comparison of various methodologies is contrasted. There is a lot of interest in studies surrounding rational function approximation. This may efficiently approximate abruptly changing functions and has many possible real-world applications. A generalized rational approximation for fractional order in the ideal fractional operator response was proposed in this research afterwards. Figure 1 illustrates the process flow diagram.

A Charef approximation method is proposed for the fractional-order transfer function in this work. Fractional-order control has mostly turned to meta-heuristic optimization methods to search for and test potential solutions to increase controller performance. The study also suggested the time responses of Find a Minimum of a Constrained (FMINCON) nonlinear multivariable function with the Mayfly optimization algorithm presented, which analyses the convergence behaviour and magnitude error metrics of the various order FO. A simulated annealing model is suggested for the generalization of the model, which increases response effectiveness for hyperparameter tuning.

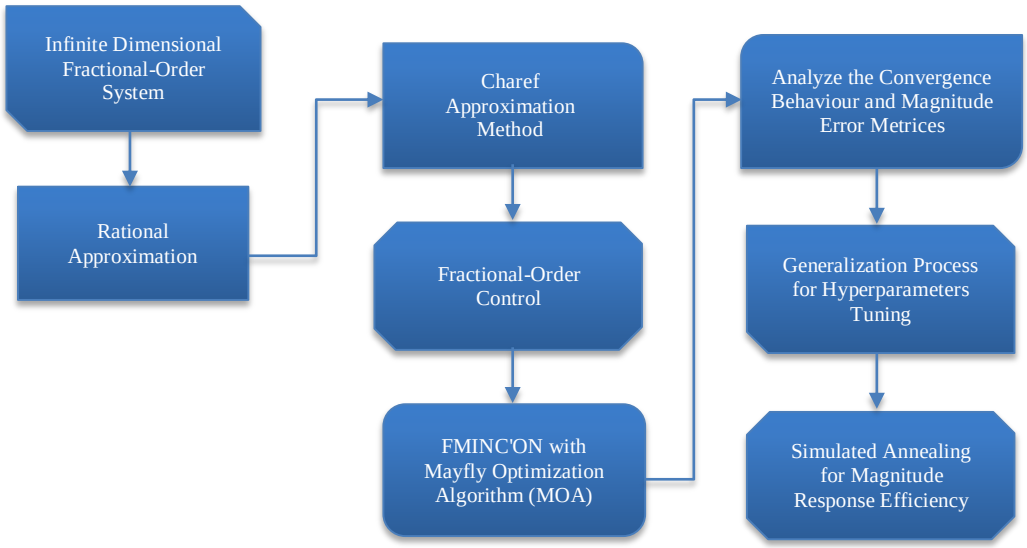

Fig. 1 Flow diagram of the proposed work

4.1. Charef Approximation Method

Integrating the Charef Approximation with optimization algorithms involves utilizing the approximation to convert fractional-order systems into a form suitable for optimization. This method allows for deriving integer-order approximants that can be manipulated using optimization techniques to improve system performance. By applying optimization algorithms, such as the Mayfly Optimization Algorithm or Simulated Annealing, the parameters of the Charef approximation can be fine-tuned, enhancing the accuracy and stability of the resulting integer-order models while preserving the essential characteristics of the original fractional-order system.

The possibility of application of the fractional order transfer function is determined by the possibility of its finite dimensionality and integer order approximation. Several authors have discussed the approximation of fractional-order transfer functions. The fractional order transfer function of an inertial plant can be approximated using the rational Charef approximation, which is presented below.

$$G(s) = \frac{1}{(Ts+1)^{\gamma}} \tag{1}$$

Where T stands for the plant's time constant and $0 < \gamma < 1$ means the fractional order. The following Equation (2) expresses the transfer function's finite-dimensional approximation.

$$G_{ch}(s) = \frac{\prod_{n=0}^{N-1}\left(1+\frac{s}{z_i}\right)}{\prod_{n=0}^{N-1}\left(1+\frac{s}{p_i}\right)} \tag{2}$$

Where N stands for the approximation's order and z_i and p_i Stand for the approximation's zeros and poles. This approximation aims to best match a plant's Bode magnitude plot to that of the approximation in a certain frequency band. The following recursive dependencies are used to calculate zeros and poles.

$$p = \frac{1}{T} \tag{3}$$

$$p_0 = p\sqrt{b} \tag{4}$$

$$z_0 = ap_0 \tag{5}$$

$$p_i = p_0(ab)^i i = 1, \dots N \tag{6}$$

$$z_i = ap_0(ab)^i \qquad i = 1, \dots N \tag{7}$$

Where, $a = 10^{\frac{\Delta}{10(1-\alpha)}}$, $b = 10^{\frac{\Delta}{10\alpha}}$, and $ab = 10^{\frac{\Delta}{10\alpha(1-\alpha)}}$. The difference between the Bode magnitude plots for the model and plant, stated in [dB], where $\Delta > 0$ determines the maximum acceptable error of the Charef approximation in a, b, and ab. It is possible to estimate the order of approximation N as follows.

$$N = Int\left(\frac{log(\omega_{max}T)}{log(ab)}\right) + 1 = Int\left(\frac{10\alpha(1-\alpha)log(\omega_{max}T)}{\Delta}\right) + 1 \tag{8}$$

Where, ω_{max} Stands for the widest frequency band that the approximation will be used. The transfer function can be represented as the following product; hence, the Bode magnitude plot of the function deals with a sum of the plots stated.

$$G(s) = G_{\alpha}(s)G_{\beta}(s) \tag{9}$$

Where the following Equation (10) and (11) can be used to express $G_{\alpha}(s)$ and $G_{\beta}(s)$.

$$G_{\alpha}(s) = \frac{1}{(T_{\alpha}s+1)^{\alpha}} \quad (10)$$

$$G_{\beta}(s) = \left(T_{\beta}s+1\right)^{\beta} = \frac{1}{\frac{1}{\left(T_{\beta}s+1\right)^{\beta}}} \quad (11)$$

Using approximations (2) to (8), the transfer function (10) can be directly approximated. Equation (12) represents its approximation as $G_{ch\alpha}(s)$.

$$G_{ch\alpha}(s) = \frac{\prod_{n\alpha=0}^{N\alpha-1}\left(1+\frac{s}{z_{n\alpha}}\right)}{\prod_{n\alpha=0}^{N\alpha}\left(1+\frac{s}{p_{n\alpha}}\right)} = \frac{L_{ch\alpha}(s)}{D_{ch\alpha}(s)} \quad (12)$$

The approximation order is equal to N_{α}. The approximation of the second factor of the transfer function is denoted by the expression (11). This suggests that the approximation for the inertial plant stated in (13) might be proposed as the inverse of this approximation.

$$G_{ch\beta}(s) = \frac{\prod_{n\beta=0}^{N\beta-1}\left(1+\frac{s}{p_{n\beta}}\right)}{\prod_{n\beta=0}^{N\beta}\left(1+\frac{s}{z_{n\beta}}\right)} = \frac{D_{ch\beta}(s)}{L_{ch\beta}(s)} \quad (13)$$

Consequently, the approximate $G_{ch}(s)$ value for the entire transfer function is described as follows.

$$G_{ch}(s) = G_{ch\alpha}(s)G_{ch\beta}(s) = \frac{L_{ch\alpha}(s)D_{ch\beta}(s)}{D_{ch\alpha}(s)L_{ch\beta}(s)} \quad (14)$$

The transfer function's numerator and denominator in Equation (14) have the same summarising order, which is equal to $N_{\alpha} + N_{\beta} - 1$. The estimation presented above is very "cautious" and describes the upper limits of inaccuracy. Although the actual error is much smaller, it can increase significantly in the presence of cancellation poles or zeros. Due to their fractional ordering, fractional systems have a significant difficulty because of their infinite dimensionality in time domain simulations when compared to regular systems. Compared to the previous model, this one uses fewer components and provides results that are more accurate when considering interest frequency. This indicates the corresponding resistor and capacitor values for the desired frequency.

4.1.1. Proportional-Integral-Derivative (PID) Fractional-Order Controllers

Researchers have established that integer-order controllers can be replaced by FO controllers. This has prompted numerous studies on the design and evaluation of these controllers. Such controllers only have one drawback: to implement them, their dynamics must be approximated. The PID fractional-order controllers are modelled in practice as high-order integer-order transfer functions. As a result, it is simple to apply the proposed methodology to other established approximations. The following Equation (15) describes the differential equation of a fractional order PID controller.

$$u(t) = k_P e(t) + k_I D_t^{-\lambda} e(t) + k_D D_t^{\delta} e(t) \quad (15)$$

The following Equation (16) is the continuous transfer function of FOPID that is computed using the Laplace transform.

$$G_c(S) = k_P + k_I S^{-\lambda} + k_D S^{\delta} \quad (16)$$

Designing a FOPID controller entails designing three parametersk_P, k_I, k_D, as well as two orders λ; δ, neither of which must be integers. A typical integer-order PID controller is produced by taking$\lambda = \mu = 1$. Evaluation of a fractional integrodifferential operation over a function is subject to several definitions. The Grünwald-Letnikov, Caputo, and Riemann-Liouville definitions are the ones that are most frequently employed in the literature. However, Equation (17) provides the Riemann-Liouville definition.

$${}_aD_b^r f(t) = \frac{1}{\Gamma(\upsilon-r)}\frac{d^{\upsilon}}{dt^{\upsilon}}\int_a^b \frac{f(\tau)}{(t-\tau)^{r-\upsilon+1}}\,d\tau \quad (17)$$

Equation (18) gives the Riemann-Liouville definition of the fractional derivative in the Laplace Transform for$(\upsilon - 1 < r < \upsilon)$.

$$L\{\,{}_aD_b^r f(t)\} = s^r L\{f(t)\} - \sum_{k=0}^{n-1} s^k\,{}_aD_b^{r-k-1} f(t)\Big|_{t=0} \quad (18)$$

For $(\upsilon - 1 < r \leq \upsilon)$, where the complex Laplace transform variable $s = \sigma + j\omega$ is used. It should be noted that the integer-order derivative's Laplace Transform is comparable to the fractional derivatives. Transfer functions can be used with the fractional order controller, which generalizes the traditional integer order PID controller. This growth may give greater flexibility to accomplish control goals.

4.2. Hybrid FMINCON-Mayfly Optimization Algorithm

The step response of Fractional Order (FO) elements often cannot be accurately approximated using frequency domain approaches alone. The research proposes a novel optimization method based on a rational approximation scheme to address this limitation, significantly enhancing step response performance without compromising frequency response accuracy. This work improves approximate FO derivative models by integrating the Mayfly Optimization Algorithm (MOA) with time responses from the Find the Minimum of a Constrained (FMINCON) nonlinear multivariable function) technique. The hybrid optimization approach facilitates parameter selection through the pathfinder algorithm, focusing on convergence behaviour and

magnitude error metrics for various order FO elements. This unique integration represents a significant contribution to the literature on fractional-order systems, offering new methodologies for improved performance.

4.2.1. FMINCON Algorithm

The Find the Minimum of Constrained (FMINCON) algorithm finds the minimum of a constrained nonlinear multivariable equation using the interior-point algorithm. The chosen approach, called "interior point", can deal with both large and small, intensive situations that are sparse. The Fmincon method can improve from NaN or INF results and compensate for the constraints throughout all iterations. For complex problems, this method can make use of some unique strategies. Figure 2 displays the flowchart for the Fmincon algorithm.

The input value for the Fmincon algorithm process contains the Active powers, Constraints, and Beginning point.x_0. Based on the provided constraints, an evaluation procedure is conducted. J Is considered as Fmincon function. The number of iterations will be increased, and newKp, Kd, Ki values will be chosen within the parameters. The current Fmincon function $J(xi)$ and the prior value $J(xi-1)$ are compared. Until the best optimal value ofKp, Kd, Ki is attained, or the iteration reaches its maximum value, the iteration will be repeated. An Integral Square Error (ISE) is thought to be the objective function. The ISE is represented by Equation (19), where $e(t)$ is the error, which is the difference between the actual and the desired pressure value.

$$ISE = \int_0^T e(t)^2 dt \tag{19}$$

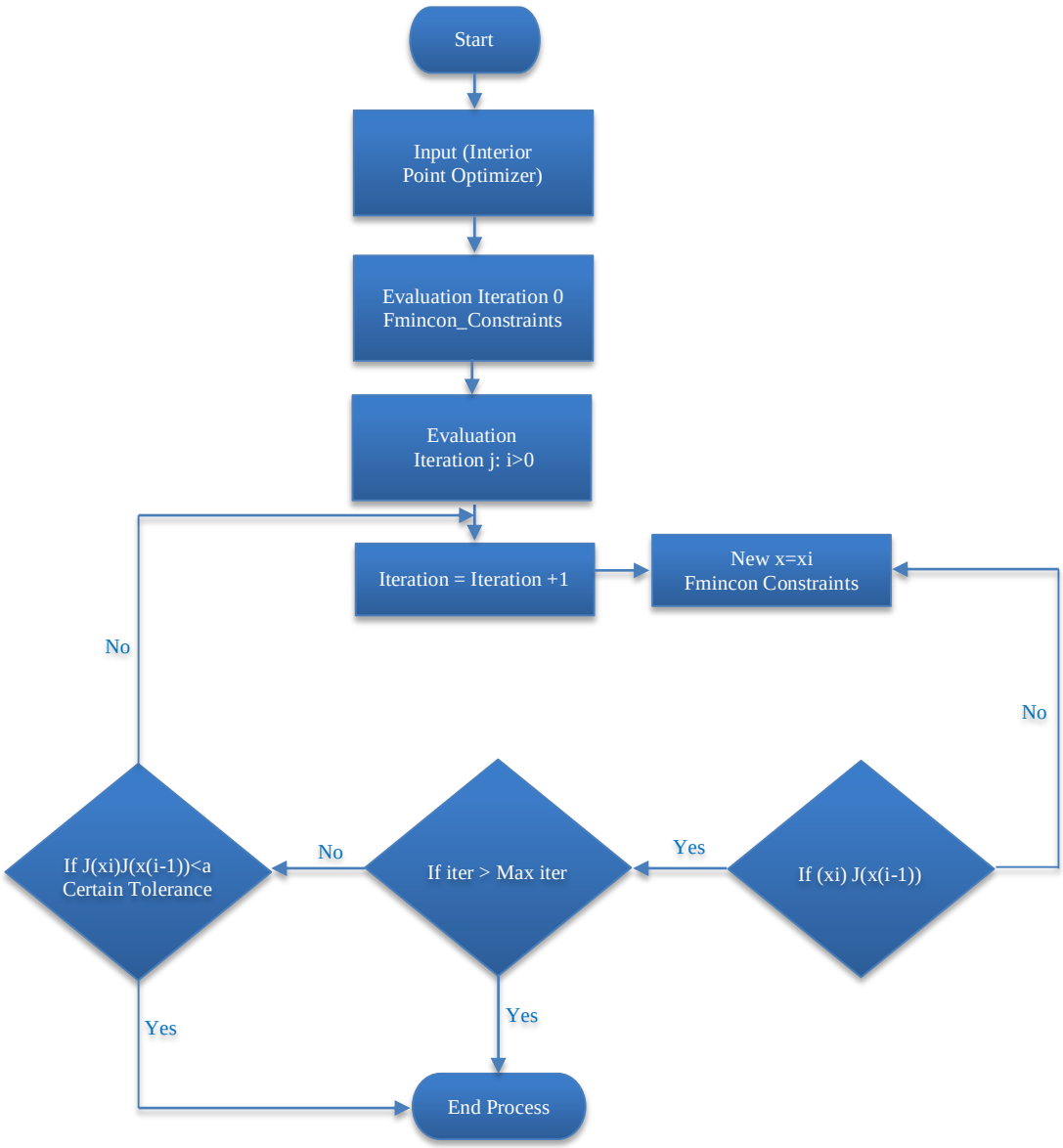

Fig. 2 Flowchart for FMINCON algorithm

The starting point is taken to be$X = (X1, X2, X3)$. Based on the ISE objective function, Equations (20) to (22) return the PID parameter values.

$$[Kp, fv1, ef1, op1, L, G, H] = f(ISE, X1, A1, b1, Aeq1, beq1, lb1, ub1, N1, O1) \quad (20)$$

$$[Ki, fv2, ef2, op2, L, G, H] = f(ISE, X2, A2, b2, Aeq2, beq2, lb2, ub2, N2, O2) \quad (21)$$

$$[Kd, fv3, ef3, op3, L, G, H] = f(ISE, X3, A3, b3, Aeq3, beq3, lb3, ub3, N3, O3) \quad (22)$$

In Equations (20) to (22), the method starts with the beginning value and uses the objective function ISE to determine the minimum value of the function. In equations (20)-(22), the final value is abbreviated asfv, the exit flag asef, the output as op, and fmincon is abbreviated as f. L Stands for the Lagrange multiplier field structure, and G for the gradient of the PID parameter's objective function. The constraints on linear inequality are represented by the matrices a and b, respectively.

The linear equality constraints matrix and vector are designated as Aeq andbeq, respectively. The PID parameters' lower and upper bounds are shown as lb andub, respectively. The value of the objective function, which is returned as a real number, is $fval$. Nevertheless, O stands for the option that returns a collection of the optimization problem, and H stands for the Hessian of the PID parameter's objective function.

Together with a structured output including information about the optimization process, FMINCON also produces a value exit flag that identifies the algorithm's exit state. In Equation (23), the Hessian of the Lagrangian is depicted.

$$H = \nabla^2 L = \nabla^2 ISE + \sum_i \lambda_i \nabla^2 C_i + \sum_j \lambda_j \nabla^2 Ceq_j \quad (23)$$

The nonlinear inequality constraint vector is denoted by$C$, and the nonlinear equality constraint vector is denoted byCeq. The Broyden-Fletcher-Goldfarb-Shanno (BFGS) technique is chosen in Hessian because it solves unconstrained nonlinear optimization problems interactively. Set typical X values that represent the distinct magnitude of the variables in the algorithm configuration. The maximum iterations in the projected conjugate iteration denote the greatest possible number of projected conjugate gradient iterations. The relative tolerance shows the projected conjugate gradient iteration's relative termination tolerance. The absolute tolerance indicates the projected conjugate gradient iteration's absolute termination tolerance. The stopping criterion indicates the algorithm's termination point. The algorithm's maximum number of iterations is indicated by the term "max iterations". The evaluations of the Max function must include most instances of the constraints and objective function. The method proceeds through numerous iterations until the best-fit values are obtained. The Mayfly Optimization Algorithm will receive the best-fit value obtained by the Fmincon method as input. The approximation FO derivative models are enhanced by the MOA. The mayfly optimization technique is given in the following subsection.

4.2.2. Mayfly Optimization Algorithm (MOA)

The Mayfly optimization method is presented as a brand-new approach to intellectual optimization. Moreover, mayfly mating and fighting behaviours had an impact on the algorithm. The system combines the main advantages of swarm intelligence and evolutionary intelligence. Despite the mayfly optimization algorithm's clear advantages in convergence speed, accuracy, and exploitation, interest in it keeps growing. Each mayfly's position in the search space suggests potential, essential key solutions to the challenging circumstances. The steps for the mayfly algorithm are given as follows.

Step 1: Initialize both the male and female mayfly populations and set the speed parameters.
Step 2: Calculate the fitness value and sort the outcomes to obtain pbest and gbest.
Step 3: Update the locations of the male and female mayflies in turn and to mate.
Step 4: Update pbest & gbest after calculating fitness.
Step 5: Verify whether the stop condition has been attained; if so, exit and output the result; otherwise, repeat steps 3 to 5.

Initiation

Create a population of males and females with initial positions of $x_i = [x_1, \dots, x_d]$ and $y_i = [y_1, \dots, y_d]$ and corresponding velocities of $v_i = [v_1, \dots, v_d]$.

Male Movement

Each mayfly modifies its position to achieve both its own best position orp_{best}, and the best position achieved by its neighboursg_{best}, which has been described as follows.

$$x_{ij}^{t+1} = x_{ij}^t + v_i^{t+1} \quad (24)$$

$$v_{ij}^{t+1} = v_{ij}^t + a_1 e^{-\beta r_p^2}\left(pbest_{ij} - x_{ij}^t\right) + a_2 e^{-\beta r_g^2}\left(gbest_{ij} - x_{ij}^t\right) \quad (25)$$

Where, a_1 and a_2 are the global and personal learning coefficients, and x_{ij}^t and v_{ij}^t are the location and velocity of agent i at dimension j and iteration$t$. The constant coefficient isβ, and the Cartesian distances r_p and r_g stand for personal and global distances, respectively. The formula for the best mayfly's velocity is$v_{ij}^{t+1} = v_{ij}^t + d * r$. Where d is the nuptial dance coefficient and r is the random value between [-1, 1].

Female Movement

A female mayfly updates its location using the following formula based on the Cartesian distance between itself and the males.

$$y_{ij}^{t+1} = y_{ij}^{t} + v_i^{t+1} \tag{26}$$

$$v_i^{t+1} = \begin{cases} v_{ij}^{t} + a_2 e^{-\beta r_{mf}^2}\left(x_{ij}^{t} - y_{ij}^{t}\right) if\ f(y_i) > f(x_i) \\ v_{ij}^{t} + fl * r\ if\ f(y_i) \le f(x_i) \end{cases} \tag{27}$$

Where, a_2 is a positive attraction coefficient and y_{ij}^{t} and v_{ij}^{t} represent the position and motion of female i at dimension j and iteration t, respectively. As opposed to this, fl is a random coefficient, r_{mf} is the Cartesian distance between males and females, and β is a fixed coefficient.

Mayfly Mating

Male and female will mate and produce two springs. The equation is shown in the following format.

$$\begin{aligned} offspring1 &= L * male + (1 - L) * female \\ offspring2 &= L * female + (1 - L) * male \end{aligned} \tag{28}$$

Where the male is a parent, and the female is a parent, L is a random number. The male population will gain one offspring, while the female population will gain the other offspring. Accordingly, the initial velocities of the offspring will be zero. Male and female candidates may be chosen at random or according to fitness.

Update Solutions

The worst solutions are swapped out for the best brand-new ones, and then$gbest$, $pbest$ are updated. Until the stop criteria are satisfied, the previous processes are repeated.

However, the Gauss distribution with an arbitrary statistic is denoted as L in Equation (24). In contrast, the tuning of the mayfly optimization initially suffers, but a weighted parameter is also included to increase this progress efficiency. In this case, the MO enhances the approximatively FO derivative models and finally addresses the multi-objective issues.

4.3. Generalization Process

Fractional calculus is identified with advantages of such kinds and it can be considered as a generalization of method to describe the characteristics, including integer-order values. To ensure convergence of the cost function and parameter values generalization of the model, selecting the appropriate batch size is crucial. There has been some research on how to decide, but there is no agreement. The study employs a hyperparameter search in practice, and the objective is to experiment with the hyperparameters to discover parameter values that minimize a cost function. Also, it was suggested in this study that the Simulated Annealing (SA) technique be improved to find the best hyperparameters with unique target values. The effectiveness and dependability of the produced model's final verification demonstrate the fractional-order optimizer's controllability.

4.3.1. Simulated Annealing

Simulated Annealing (SA) is a probabilistic implementation of the Metropolis algorithm that accepts non-improving movements. In a single-objective SA, the neighbourhood of the present solution X, which is defined as all the solutions that can be reached by a single move from X, is used to select a new solution, X'. The representation chosen to encode a workable solution determines the moves that can be made in a SA. The problem domain, on the other hand, has a significant impact on solution representation. For a minimization issue, X' is allowed if its objective function value is less than X. If X' is worse than X, it is accepted with a probability p_{acc}, grounded on the objective function's worsening amount and the system's current temperature and is calculated as follows: $p_{acc} = min\{1, exp(-\Delta F/T_{cur})\}$. Where ΔF is the objective function's worsening amount and T_{cur} is the system's current temperature.

Simulated annealing prevents the Particles, in this case, from becoming stuck in regionally optimal solutions. It uses a probabilistic method, where the algorithm initially allows the particles to accept sub-optimal solutions with a high likelihood, assisting them in leaving local optimum locations (minimums or maximums, depending on the nature of the problem). The algorithm will gradually reduce the likelihood of accepting less-than-ideal solutions. The local best solution and the global best solution, in addition to the Simulated Annealing acceptance criteria, will still influence the particles' velocity and direction. The Simulated Annealing acceptance criterion will be applied to the particle's local best solution. The simulated annealing algorithm for the suggested method is illustrated in Table 1 below.

Table 1. Simulated annealing algorithm

Algorithm 1: Simulated Annealing-Based Acceptance Criteria
Input: Initial solution, initial position, initial metric, maximum number of iteration
Output: The best solution
if current Metric>previous Metric then
previous metric = current metric
previous position = current position
if current Metric > local Best Metric, then
local Best Metric = current Metric
local Best Position = Current Position
end
else
random number = Get a random number between 0 and 1
metric Difference = current metric – previous metric
threshold = $e^{\beta * metricDifference/T}$

if the random Number < threshold, then
previous position = current position
previous metric = current metric
end
end
if epoch $mod\ k == 0$ then
$T = \alpha * T$
end

In method 1, "T" stands for the present "temperature," which estimates the likelihood that less-than-ideal solutions will be accepted. The acceptance probability will decrease as the temperature drops after k epochs. The scaling factor for the temperature is α, and the user-adjustable normalizing constant is β, with a default value of 1.3.

The error rate is an objective that the SA algorithm takes into account in this study, and it only accepts a new solution X' if it is superior to the current answer X in terms of this single objective value. The SA chooses the option with the fewer FLOPs, even if X and X' have the same error rate. In "Local Moves," the composite motion produced X' is defined. Use a real-time initial temperature selection approach to defineT_{init}. This method does not calculate p_{acc} using the equation$p_{acc} = min\{1, exp(-\Delta F/T_{cur})\}$. The acceptance of the worsening moves is specified as having a predetermined beginning probability value, which is advised to be 0.5. Where, ΔF_{ave} is the average deteriorating penalty amount determined by carrying out a brief "burn-in" phase and is then used to calculate T_{init} as $-(\Delta F_{ave}/(ln(p_{acc})))$. T_{final} is defined using a similar real-time temperature adjustment method. The SA stopping criterion in this study is specified by the total iteration budget, and the number of inner and outer iterations is determined by the cooling strategy and this iteration budget. However, each position vector component is considered as a value for a hyper-parameter of a particular method while evaluating the particle position.

4.4. Comparison of Proposed Method with Existing Models

The proposed Charef rational approximation method for fractional-order systems offers distinct advantages over existing models, particularly in enhancing time response accuracy and stability. Unlike traditional integer-order models, which can struggle with the complexities of fractional dynamics, the Charef method employs a pole and zero model that allows for greater flexibility in system representation, with poles that are not constrained by the order of the integrator. This flexibility enables better alignment with real-world system behaviours, especially when combined with optimization techniques like the Mayfly Optimization Algorithm (MOA), which further refines the time responses of FMINCON-based fractional-order derivative models. Compared to other fractional-order modelling approaches, the proposed method demonstrates superior performance in approximating system dynamics, as evidenced by numerical examples highlighting its broad applicability and acceptable accuracy, making it a valuable tool for engineers and researchers in various fields. The proposed Charef rational approximation model can be applied in real-world scenarios, such as optimizing temperature control in chemical reactors, leading to improved response times and stability. In robotics, it enhances motion control for robotic arms, enabling smoother and more precise trajectory tracking. These case studies demonstrate the model's effectiveness in practical applications by providing superior time response accuracy and adaptability in complex systems.

4.4.1. Limitations of the Current Study

The current study utilizing the Charef Approximation Method for fractional-order system models, in conjunction with the hybrid FMINCON-Mayfly Optimization Algorithm, has certain limitations. While the approach demonstrates effectiveness across various applications, it may not fully capture the complexities of highly nonlinear systems or varying dynamic conditions, which could affect performance. Additionally, the reliance on numerical examples limits the generalizability of the findings; further validation through experimental studies is necessary. Lastly, the computational efficiency of the proposed method, particularly in real-time applications, warrants further exploration to determine its practicality in dynamic environments.

5. Experimentation and Results Discussion

A fractional order transfer function with MOA-based FOPID control is made using MATLAB software. This Matlab model includes the magnetizing inductor. This model for the suggested MOA-FOPID control consists of a voltage control loop based on MA at the external and a current control loop based on FOPID at the internal. For the specified output power and input voltage, 50 kHz is chosen as the switching frequency to fulfil the resonant converter's functions.

The converter operates with an input voltage of 100 volts DC and an output voltage kept at a level close to 5 volts DC. Harmonic distortions and power factors are not considered because the suggested method's input operates in DC. Table 2 depicts the simulation system configuration for the proposed work.

Table 2. Simulation system configuration

MATLAB	**Version R2021a**
Operation System	Windows 10 Home
Memory Capacity	6GB DDR3
Processor	Intel Core i5 @ 3.5GHz
Simulation Time	10.190 seconds

The relevant converters' input and output requirements are specifically considered. It has been evaluated as a standard value. These converters function at maximum efficiency. The details of the parameter values, components, and units will be utilized in the proposed converter. The MOA procedure is simulated using a MATLAB script, which starts with 100 mayflies (as Nm=100).

The dimension of the position vector changes at each time step as a result of this algorithm's determination of the duty ratio value. Every repetition includes a 0.01-second pause. Using random vectors produced by the Gauss distribution G, the location vectors are updated. Using the results of simulations, the frequency response and the time response produced by the approximation approaches have then been compared. Numerical examples are provided to demonstrate the method's broad application and to demonstrate the acceptable accuracy for approximations.

5.1. Numerical Examples for Charef Approximation

Example 1: Let's use the following transfer function as the first example.

$$G(s) = \frac{(5s+1)^{0.5}}{(47s+1)^{0.5}} \quad (29)$$

The aforementioned transfer function's approximation will be constructed for a pulsation range of 10^{-3} [sec^{-1}], with a maximum error $\Delta = 1$ [dB].

$$\exists n_\alpha = 0 \ldots N_\alpha, \exists n_\beta = 0 \ldots N_\beta : z_{n\alpha} = z_{n\beta} \vee p_{n\alpha} = p_{n\beta} \quad (30)$$

Calculate the order of the two components of the approximation using this equation; in other words, $N_\alpha = 5$, $N_\beta = 6$.

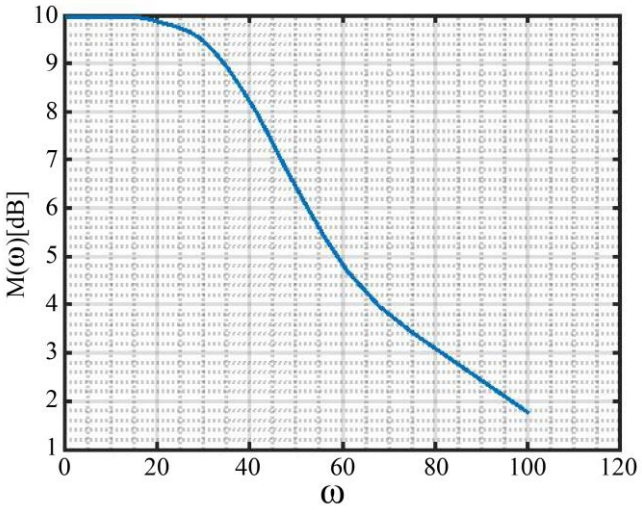

Fig. 3 Exact bode magnitude plot for the transfer function

Figure 3 depicts the precise Bode magnitude plots for the plant described by (29), respectively. These plots were created using MATLAB/SIMULINK. However, the Bode magnitude plots are exact and approximated, as illustrated in Figure 4.

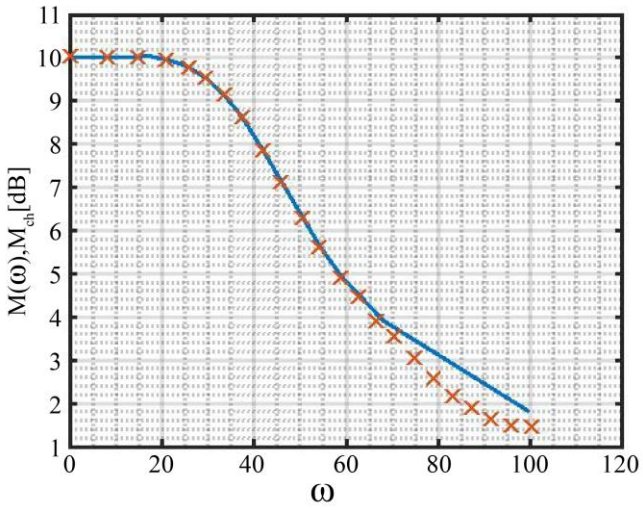

Fig. 4 Exact and approximated bode magnitude plots for the transfer function

The largest error in the approximation (Δ_s) for this situation is less than 0.06 [dB]. Looking at the graphs in Figure 4, it can be concluded that the approximation is accurate, and its maximum error is not more than 0.06 [dB]. This error is much smaller than the maximum estimated error. The maximum value of the approximation error Δ_s (ω) in this case is 1.3 [dB]. After comparing these results, the cancellation poles or zeros in the proposed approximation affect its performance negatively.

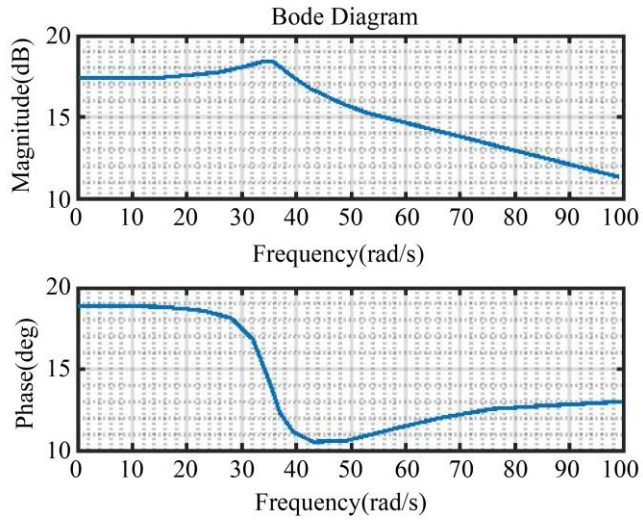

Fig. 5 Bode diagrams of the original and reduced-order fopid controllers

Figure 5 displays the Bode diagrams of the original and simplified control systems, showing very similar behaviours in the relevant frequency range. To highlight the benefits of

the suggested FOPID controller, a PID controller is also designed using the same approach. The system's frequency response where the desired phase margin $\varphi_d \approx 60°$ can be corroborated

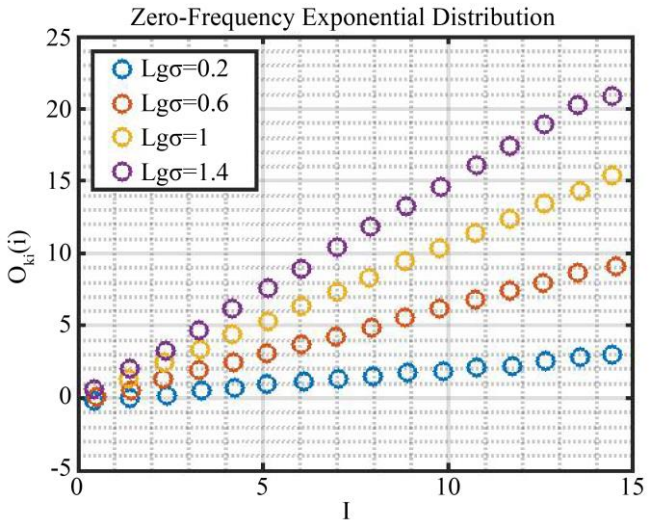

Fig. 6 Zero-frequency exponential distribution graph

Figure 6 illustrates the distribution of zero-frequency exponential distribution for overtime, which closely resembles an exponential distribution. In this context, the single parameter 'l' represents the mean value, with l being 1.095. The Lg values for 0.2, 0.6, 1, and 1.4 demonstrate a good match between the exponential distribution and the measured frequency of overtime hours. Consequently, an exponential distribution can be used to describe overtime duration, with the average overtime duration being the only parameter to consider.

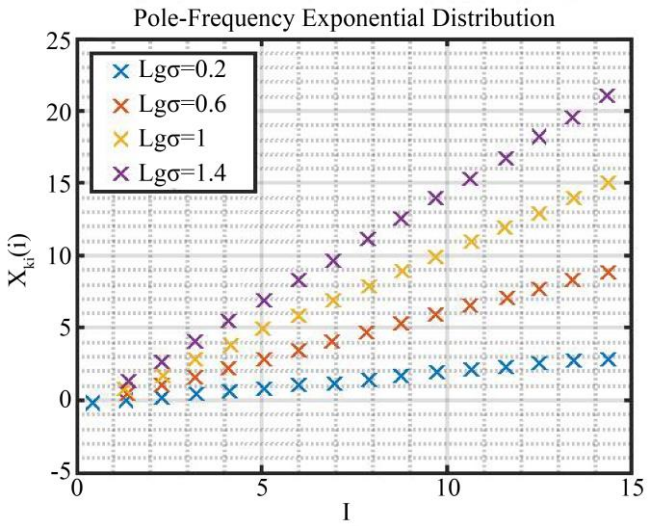

Fig. 7 Pole frequency exponential distribution graph

In Figure 7, the pole frequency exponential distribution graph is depicted. When σ is set to 1.25, the two poles are extremely close, rendering the dominant pole approximation invalid, as the precise response (magenta) does not align with the approximations featuring a first-order pole dominating (red and blue lines). The step response for this scenario exhibits a distinct time scale compared to the previous two cases. When σ is 10, the complex poles dominate, causing the system to behave approximately like a second-order system. The real pole (associated with the swift part of the response) can be disregarded in this scenario.

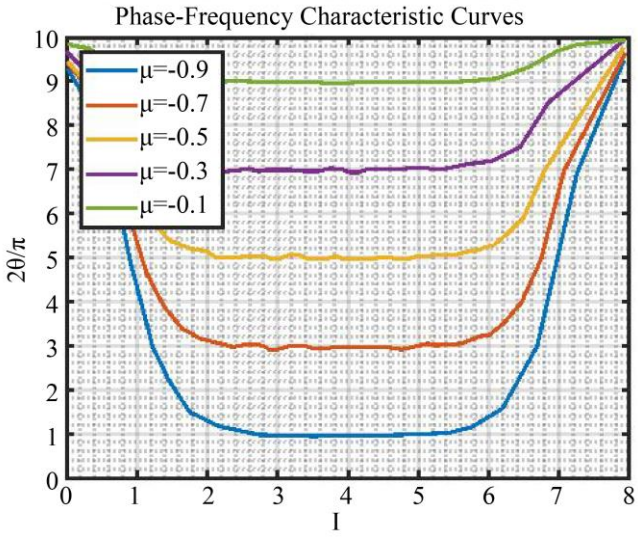

Fig. 8 Phase frequency characteristics curve

In Figure 8, the phase frequency characteristics curve of the proposed work is displayed. This figure illustrates the vibration response and phase attributes at various mode frequencies, with the sense mode set to 5000. A notable observation is that when the two-mode frequencies align, the vibratory response of the sense mode reaches its peak, while the phase delay also experiences a significant shift.

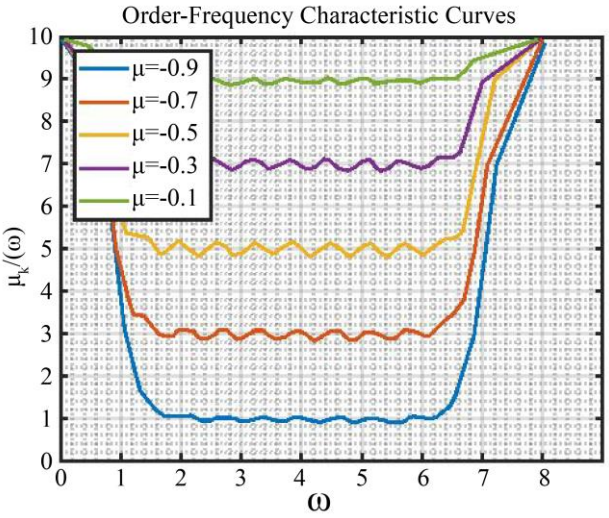

Fig. 9 Ordered-frequency characteristics curve

The Ordered-Frequency Characteristics Curve of the proposed work is presented in Figure 9. It is measured for the μ values of 0.1, 0.3, 0.5, 0.7, and 0.7. Selecting the control gain value $p = -0.05$, the frequency amplitude curve that by adjusting different time delays, a better control effect can be obtained, and the peak value of the response can be significantly reduced

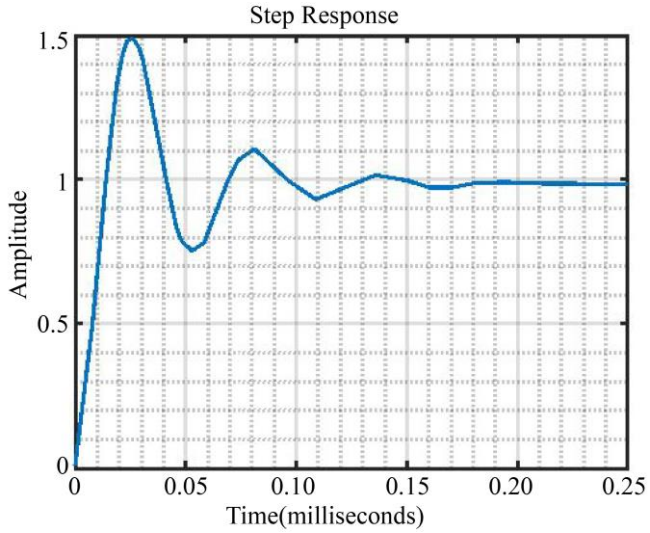

Fig. 10 Closed-loop step response of fractional order transfer function

In Figure 10, the closed-loop step response of the PID converter transfer function with a controller is shown. The effectiveness of the proposed structure in regulating output voltage in buck converters can be corroborated. Response velocity can be characterized by its time-related performance parameters rise time $t_r = 8.75\mu s$, peak time $t_r = 21.29\mu s$ and settling time $t_s = 74.17\ \mu s$, respectively.

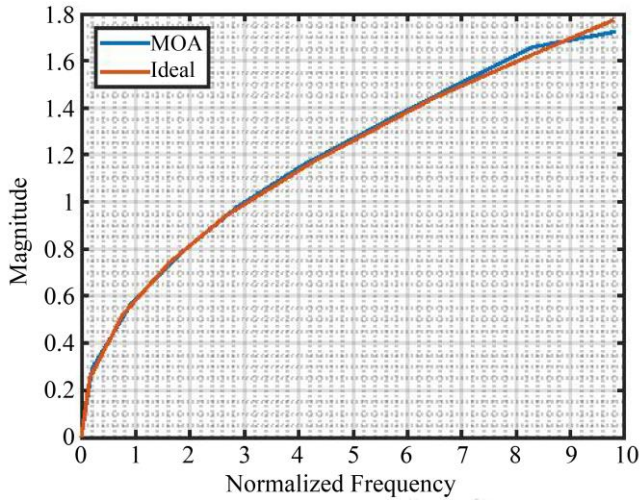

Fig. 11 Magnitude response graph for the proposed method

Figure 11 reveals the magnitude of the response to the proposed methodology. The roll-off rate is the rate of change of the output of the filter versus frequency. It is expressed as a loss per decade or octave, a two-time increase in frequency. The magnitude response for the MOA reveals the best performance value and achieves optimal results.

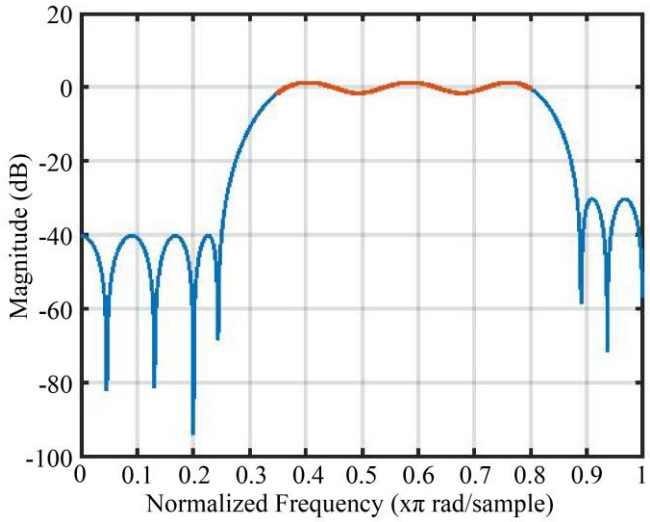

Fig. 12 Frequency responses of PID controller

Figure 12 shows the Frequency Responses graph for the proposed controller. The parameters provide a frequency response comparable to the one of the PID in the range $10 \div 1000\,rad/s$, but with different magnitude slopes and asymptotic phase values outside this range.

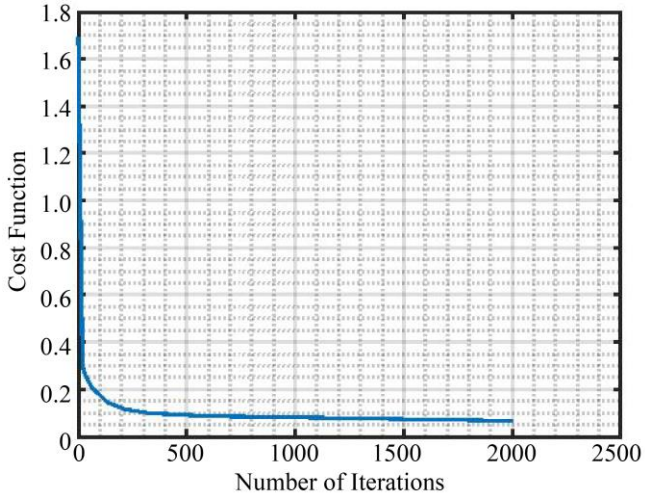

Fig. 13 Cost function for the proposed work

Figure 13 shows the output plot for the cost function of the work. In which the plot is produced between several iterations and the cost. From the graph, there is a constant decrement in cost for the increased no. of iterations corresponding to the number of iterations being 2000, and it measures the cost function value as approximately equal to 0.1, respectively.

Table 3. Performance values of the proposed method

Parameters	Values
Zero-Frequency Exponential Distribution	21
Pole Frequency Exponential Distribution	21.5
Phase Frequency	9.8
Ordered-Frequency	9.7
Step Response	0.98
Magnitude Response	1.73
Frequency Responses	0.2
Cost Function	0.6

Table 3 reveals the performance values for the proposed work, which consist of zero and pole-frequency exponential distribution values of 21 and 21.5. However, phase and ordered frequency values are 9.8 and 9.7. The step response, magnitude response and frequency responses are 0.98, 1.73 and 0.2, and the cost function values for the proposed work are 0.6, respectively.

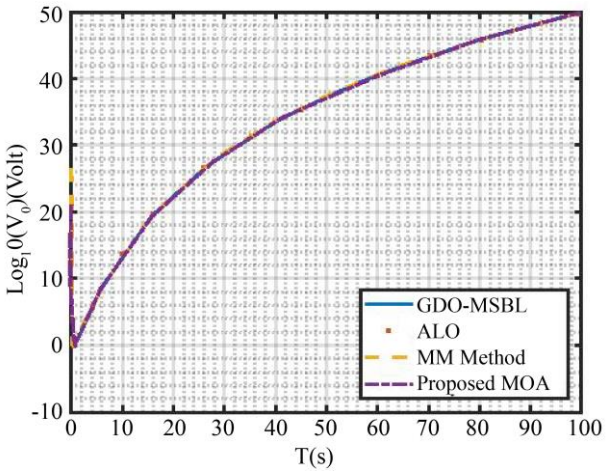

Fig. 14 Comparative step response of fractional-order transfer function

The comparative step response of the proposed MOA algorithm is compared with the existing three models provided in Figure 14. The comparison methods are GDO-MSBL, ALO, and MM methods, respectively. The performance of the proposed DE approach with model reduction allows a very competitive level of performance when compared to the ALO method. Obviously, the order reduction implies a loss of performance, but the accuracy of the MOA algorithm permits maintaining a good approximation, respectively. Table 4 reveals the comparison table for step response; it contains the proposed method values along with the existing GDO-MSBL, ALO, and MM Methods. While compared to these existing methods, the proposed method produces higher performance value. However, the step response for the proposed method is 49.98; accordingly, the other existing method produces lower values than this method, which are 49.2, 49.64, and 49.7, respectively.

Table 4. Comparison table for step response

	T (s)				
Techniques	**20**	**40**	**60**	**80**	**100**
GDO-MSBL	21.9	35.75	40.64	46.08	49.2
ALO	22.1	35.8	40.7	46.1	49.64
MM Method	22.4	36	40.9	46.3	49.7
Proposed MOA	22.5	36.1	41	46.4	49.98

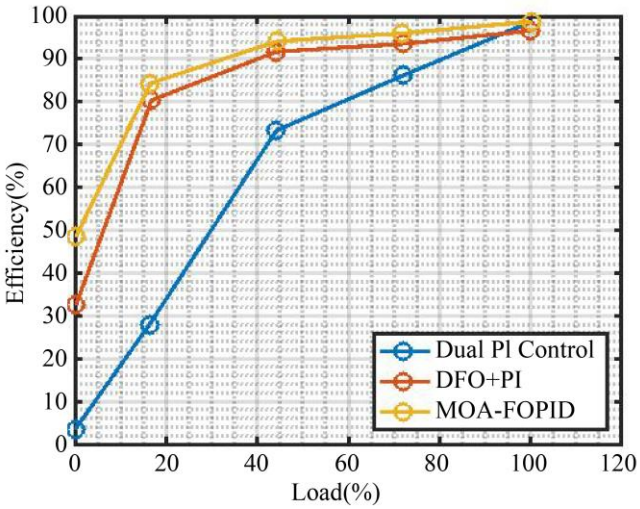

Fig. 15 Comparison graph of efficiency for different loads

Figure 15 shows the efficiency comparisons against different load percentages. This graph indicates the efficiency drop when there is a variation in the load that crosses the control limit of the corresponding controllers. The Dual PI control can able to achieve high-efficiency load only. Whereas, in DFO and PI control models, it outperforms the best Dual PI work. The control range of the MOA-FOPID converter can be evaluated with the help of input inductor value and is evaluated particularly for input and output parameters within their specific range. In MOA-FOPID control, it executed that the performance can be much better than both the conventional works with linear steadiness and also greater efficiency over the load variations.

Table 5. Comparison table for efficiency

	Load (%)				
Techniques	**20**	**40**	**60**	**80**	**100**
Dual PI Control	33.5	66	80.1	89.6	98.6
DFO+PI	81	90	92.5	94	97.5
Proposed (MOA-FOPID)	85.8	92.1	95.9	96	99.4

Table 5 showcases the comparison results for efficiency, featuring the proposed method alongside the established Dual PI Control and DFO-PI techniques. The proposed method outperforms the others, boasting an efficiency of 99.4%. In contrast, the existing methods exhibit lower efficiencies of 98.65% (Dual PI Control) and 97.5% (DFO-PI), respectively.

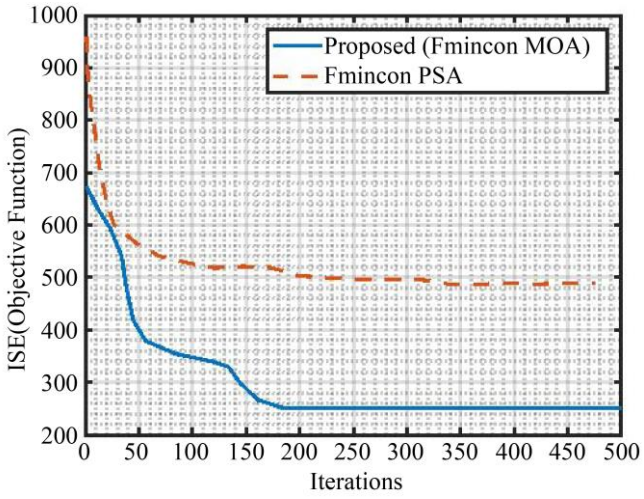

Fig. 16 Convergence comparison graph (integral squared error)

Figure 16 showcases the comparison results for the convergence diagram, featuring the proposed Fmincon-MOA algorithm versus the existing Fmincon-PS algorithm. The optimization problem's progression towards the optimal solution is visualized through this convergence graph. As depicted in Figure 16, the MOA-based FOPID algorithm initially exhibits a notably faster convergence rate than the hybrid Fmincon pattern search algorithm. Compared to the proposed fmincon MOA algorithm and a hybrid Fmincon pattern search algorithm, the fmincon MOA algorithm achieves a 38% reduction in average error at iteration 200. This significant improvement has the potential to enhance the convergence rate substantially.

Table 6. Comparison results for convergence graph

	Iterations				
Techniques	**50**	**100**	**150**	**200**	**500**
Fmincon PSA	560	523	520	500	507
Proposed (Fmincon MOA)	400	344	284	250	257

Table 6 compares convergence graphs, highlighting that the proposed method achieves a lower error rate. Specifically, it records errors of 344 (iteration 100) and 257 (iteration 500). In contrast, the existing Fmincon PSA method yields higher error values of 523 (iteration 100) and 507 (iteration 500). This demonstrates that the proposed method delivers a more enhanced performance by exhibiting a reduced error rate compared to existing techniques.

6. Research Conclusion

In recent years, fractional calculus has gained prominence due to its applications in solving various engineering problems. This work focuses on analyzing a rational approximation of the infinite-dimensional Fractional-Order System (FOS) using the Charef approximation method. The FMINCON-based Mayfly Optimization algorithm is employed to improve approximate FO derivative models to enhance controller performance. The study also examines the Simulated Annealing (SA) algorithm for determining optimal hyperparameters with custom target values. The proposed fractional-order optimizer demonstrates effective controllability. The results of the improved approximate FO model obtained using FMINCON-MOA are compared with those of approximate Fmincon PSA models for popular FO approximation methods. MATLAB software is utilized for the optimization process. The derived mathematical model is implemented in a program based on the required algorithm. The simulation results validate the magnitude response efficiency and stability of the proposed different order FO, surpassing some recently published research papers. To clarify the study and results, the paper presents the details of the proposed FMINCON-MOA method as an example. The proposed method is compared with other existing techniques like GDO-MSBL, ALO,

MM, and dual PI Controllers. Comparisons of time and frequency responses confirm that the proposed method has successfully improved time responses without affecting the frequency response negatively. The study also compares the performance of the approximation obtained using the optimization technique with the ideal frequency response of the system under consideration. The results of the trials show that the FOPID parameters are optimized with the support of the modified Mayfly algorithm. This regulating system enhances dynamic performance compared to other well-known particle search techniques, resulting in improved system performance by reducing undesired elements at specific frequencies and obtaining the desired response faster than another existing method.

References

[1] Rashid Nawaz et al., "An Extension of Optimal Auxiliary Function Method to Fractional Order High Dimensional Equations," *Alexandria Engineering Journal*, vol. 60, no. 5, pp. 4809-4818, 2021. [CrossRef] [Google Scholar] [Publisher Link]

[2] Esteban Tlelo-Cuautle et al., *Optimization of Integer/Fractional Order Chaotic Systems by Metaheuristics and their Electronic Realization*, 1st ed., CRC Press, pp. 1-266, 2021. [CrossRef] [Google Scholar] [Publisher Link]

[3] Yashveer Kumar, and Vineet Kumar Singh, "Computational Approach Based on Wavelets for Financial Mathematical Model Governed by Distributed Order Fractional Differential Equation," *Mathematics and Computers in Simulation*, vol. 190, pp. 531-569, 2021. [CrossRef] [Google Scholar] [Publisher Link]

[4] Sania Qureshi, and Rashid Jan, "Modeling of Measles Epidemic with Optimized Fractional Order under Caputo Differential Operator," *Chaos, Solitons & Fractals*, vol. 145, 2021. [CrossRef] [Google Scholar] [Publisher Link]

[5] Shibendu Mahata et al., "A Fractional-Order Transitional Butterworth-Butterworth Filter and Its Experimental Validation," *IEEE Access*, vol. 9, pp. 129521-129527, 2021. [CrossRef] [Google Scholar] [Publisher Link]

[6] J.F. Gómez-Aguilar, and Abdon Atangana, "New Chaotic Attractors: Application of Fractal-Fractional Differentiation and Integration," *Mathematical Methods in the Applied Sciences*, vol. 44, no. 4, pp. 3036-3065, 2021. [CrossRef] [Google Scholar] [Publisher Link]

[7] Chandrali Baishya, and P. Veeresha, "Laguerre Polynomial-Based Operational Matrix of Integration for Solving Fractional Differential Equations with Non-Singular Kernel," *Proceedings of the Royal Society A*, vol. 477, no. 2253, pp. 1-19, 2021. [CrossRef] [Google Scholar] [Publisher Link]

[8] M.S. Hashemi et al., "Fractional Order Alpert Multiwavelets for Discretizing Delay Fractional Differential Equation of Pantograph Type," *Applied Numerical Mathematics*, vol. 170, pp. 1-13, 2021. [CrossRef] [Google Scholar] [Publisher Link]

[9] Mengxi Tan et al., "High Bandwidth Temporal RF Photonic Signal Processing with Kerr Micro-Combs: Integration, Fractional Differentiation and Hilbert Transforms," *Advances in Physics X*, vol. 6, no. 1, pp. 1-42, 2021. [CrossRef] [Google Scholar] [Publisher Link]

[10] Andriy Lozynskyy et al., "Application of Fractional-Order Calculus to Improve the Mathematical Model of a Two-Mass System with a Long Shaft," *Energies*, vol. 14, no. 7, pp. 1-15, 2021. [CrossRef] [Google Scholar] [Publisher Link]

[11] Amirthayogam Gnanasekaran, Anbu Ananth Chinnasamy, and Elango Parasuraman, "Analyzing the QoS Prediction for Web Service Recommendation Using Time Series Forecasting with Deep Learning Techniques," *Concurrency and Computation: Practice and Experience*, vol. 34, no. 28, 2022. [CrossRef] [Google Scholar] [Publisher Link]

[12] Guessas Laarem, "A New 4-D Hyper Chaotic System Generated from the 3-D Rösslor Chaotic System, Dynamical Analysis, Chaos Stabilization via an Optimized Linear Feedback Control, it's Fractional Order Model and Chaos Synchronization Using Optimized Fractional Order Sliding Mode Control," *Chaos, Solitons & Fractals*, vol. 152, 2021. [CrossRef] [Google Scholar] [Publisher Link]

[13] Paluri Krishna Veni, and Ashish Gupta, "Acne Assessment and Grading: Challenges and Opportunity," *2023 2nd International Conference on Computational Systems and Communication*, Thiruvananthapuram, India, pp. 1-5, 2023. [CrossRef] [Google Scholar] [Publisher Link]

[14] Saleh Masoud Abdallah Altbawi et al., "Optimal Design of Fractional Order PID Controller Based Automatic Voltage Regulator System Using Gradient-Based Optimization Algorithm," *Journal of King Saud University - Engineering Sciences*, vol. 36, no. 1, pp. 32-44, 2021. [CrossRef] [Google Scholar] [Publisher Link]

[15] A. Venkata Ramana, and E. Kesavulu Reddy, "OCCSR: Document Classification by Order of Context, Concept and Semantic Relations," *Indian Journal of Science and Technology*, vol. 8, no. 30, pp. 1-8, 2015. [CrossRef] [Google Scholar] [Publisher Link]

[16] Abdul Latif et al., "A Review on Fractional Order (FO) Controllers' Optimization for Load Frequency Stabilization in Power Networks," *Energy Reports*, vol. 7, pp. 4009-4021, 2021. [CrossRef] [Google Scholar] [Publisher Link]

[17] Vanchinathan Kumarasamy, Valluvan Karumanchetty Thottam Ramasamy, and Gnanavel Chinnaraj, "Systematic Design of Multi-Objective Enhanced Genetic Algorithm Optimized Fractional Order PID Controller for Sensorless Brushless DC Motor Drive," *Circuit World*, vol. 48, no. 4, pp. 479-492, 2021. [CrossRef] [Google Scholar] [Publisher Link]

[18] S. Karthik et al., "Crypto AI: Digital Nostalgic Art Generation Using GAN and Creation of NFT Using Blockchain," *Journal of Emerging Technologies and Innovative Research*, vol. 9, no. 7, pp. 217-220, 2024. [Google Scholar] [Publisher Link]

[19] Rafał Stanisławski, Marek Rydel, and Zhixiong Li, "A New Reduced-Order Implementation of Discrete-Time Fractional-Order PID Controller," *IEEE Access*, vol. 10, pp. 17417-17429, 2022. [CrossRef] [Google Scholar] [Publisher Link]

[20] Lokesh S. Khedekar, "Strength of Data Matrix Image Over Analysis and Design of Exam Processing System," *2023 IEEE 8th International Conference for Convergence in Technology (I2CT)*, Lonavla, India, pp. 1-4, 2023. [CrossRef] [Google Scholar] [Publisher Link]

[21] Norelys Aguila-Camacho, and Javier A. Gallegos, "Error-Based Switched Fractional Order Model Reference Adaptive Control for MIMO Linear Time Invariant Systems," *Fractal and Fractional*, vol. 8, no. 2, pp. 1-21, 2024. [CrossRef] [Google Scholar] [Publisher Link]

[22] Martin Alejandro Valencia-Ponce et al., "Integrated Circuit Design of Fractional-Order Chaotic Systems Optimized by Metaheuristics," *Electronics*, vol. 12, no. 2, pp. 1-18, 2023. [CrossRef] [Google Scholar] [Publisher Link]

[23] Abdelfatah Charef, and Samir Ladaci, "Analog Realization and Numerical Evaluation of the Variable Fractional-Order Integrator $I^{\alpha(t)}$," *IFAC-PapersOnLine*, vol. 58, no. 12, pp. 7-12, 2024. [CrossRef] [Google Scholar] [Publisher Link]

[24] Khalfa Bettou, and Abdelfatah Charef, "Fractional Order $PI^{\lambda}D^{\mu}A$ Controller Design Based on Bode's Ideal Function," *Archives of Control Sciences*, vol. 33, no. 2, pp. 425-458, 2023. [CrossRef] [Google Scholar] [Publisher Link]

[25] A. Lassoued, F. Nazarimehr, and O. Boubaker, "Dynamics and Circuit Simulation of a Fractional-Order Hyperchaotic System," *Scientia Iranica*, vol. 30, no. 2, pp. 507-517, 2023. [CrossRef] [Google Scholar] [Publisher Link]

[26] Sudheer Adigintla, and Mohan V. Aware, "Improved Constant Phase Fractional Order Approximation Method for Induction Motor FOPI Speed Controller," *International Journal of Circuit Theory and Applications*, vol. 51, no. 3, pp. 1069-1091, 2023. [CrossRef] [Google Scholar] [Publisher Link]

[27] Bala Bhaskar Duddeti, "Approximation of Fractional-Order Systems Using Balanced Truncation with Assured Steady-State Gain," *Circuits, Systems, and Signal Processing*, vol. 42, pp. 5893-5923, 2023. [CrossRef] [Google Scholar] [Publisher Link]

[28] Djamel Boucherma et al., "A New Approximate Solution of the Fractional Trigonometric Functions of Commensurate Order to a Regular Linear System," *Indonesian Journal of Electrical Engineering and Computer Science*, vol. 33, no. 2, pp. 879-887, 2024. [CrossRef] [Google Scholar] [Publisher Link]

[29] Salma Emad et al., "A Study on Fractional Power-Law Applications and Approximations," *Electronics*, vol. 13, no. 3, pp. 1-22, 2024. [CrossRef] [Google Scholar] [Publisher Link]

[30] Ali Yüce, "An Approximation Method for Fractional-Order Models Using Quadratic Systems and Equilibrium Optimizer," *Fractal and Fractional*, vol. 7, no. 6, pp. 1-21, 2023. [CrossRef] [Google Scholar] [Publisher Link]